Two-Dimensional Transpiration-Cooled Nosetip

P. J. SCHNEIDER,* R. E. MAURER,† AND M. G. STRAPP‡
Lockheed Missiles & Space Company, Sunnyvale, Calif.

An analysis is given for active transpiration cooling of re-entry-vehicle nosetips. Porous-wall coolant flow and matrix/coolant energy exchange in this application are strongly two-dimensional owing to thick-wall construction and large external streamwise pressure gradients. A steady-state calculation scheme and associated digital computer code are described for design analysis of such a nosetip considering axisymmetric two-dimensional wall geometry (zero angle of attack), variable properties, and large flow rates of an incompressible coolant supplied by a single plenum chamber. The wall solution is coupled to the heating environment by a simplified exit-surface energy balance. A design sequence is illustrated by calculating a water-cooled nosetip of nonuniform wall thickness and taylored permeability distribution designed to survive re-entry without coolant starvation, undercooling or excessive overcooling. The magnitudes of second-order inertial and transient effects in the reentry example are assessed by means of an equivalent one-dimensional transient solution. The conventional one-dimensional theory is found to be nonconservative with respect to coolant plenum pressure requirements.

Nomenclature

c,c_c = matrix and coolant specific heats, Btu/lb-°F
div = divergence
ΔE = surface energy balance, Btu/sec-ft²
grad = gradient
H = enthalpy, Btu/lb
h_w = unit surface conductance (external), lb/sec-ft²
h' = volumetric surface conductance (internal), Btu/sec-ft³-°F
k,k_c = matrix and coolant thermal conductivities, Btu/sec-ft-°F
$\bar{M}$ = mean molecular weight, lb/mole
m = coolant mass (total), lb
$\dot{m}$ = coolant mass flow rate, lb/sec-ft²
P = porosity (pore volume per total volume)
Pr_c = coolant Prandtl number = $c_c\mu_c/k_c$
p = pressure, atm
q = heat rate, Btu/sec-ft²
R = radial coordinate
Re_c = coolant Reynolds number = $(\dot{m}/\mu_c)(\beta/\alpha)$
S = distance along exit surface, ft
St_c = coolant Stanton number = $(h'/\dot{m}c_c)(\beta/\alpha)Pr_c^{2/3}$
s = internal matrix surface area per unit solid volume, 1/ft
T,t = matrix and coolant temperatures, °F
u = coolant velocity, ft/sec
x,y = rectangular coordinates
z = normal coordinate (measured from inner surface)
α = viscous resistance coefficient, 1/ft²
β = inertial resistance coefficient, 1/ft
Γ = matrix permeability, ft²
δ = matrix thickness, ft
ϵ = emittance (external)
θ = time, sec
μ_c = coolant viscosity, lb/sec-ft
ρ,ρ_c = matrix and coolant densities, lb/ft³
σ = Stefan-Boltzmann constant = 14.7×10^{-14}, Btu/sec-ft²-°R⁴
ϕ = azimuthal angle, deg

Subscripts

a,c = air and coolant
cw = cold wall
l = liquid
N = nose
n = normal
o = nonblowing
p = plenum
r = recovery
req = required
stag = stagnation point
t = tangential
v = vapor
w = wall surface (exit)

Introduction

ACTIVE transpiration cooling can be used to eliminate ablation and shape change of re-entry-vehicle nosetips. Figure 1a shows the stagnation-point recession and unacceptable shape change that can occur in hyperthermal ground tests when the nosetip is constructed of a passive material. Figure 1b illustrates, by contrast, the shape stability that results when the nosetip is porous and cooled by transpiration of water over its forward spherical face.

Active transpiration cooling of small-radius nosetips exposed to hypervelocity re-entry entails a number of important

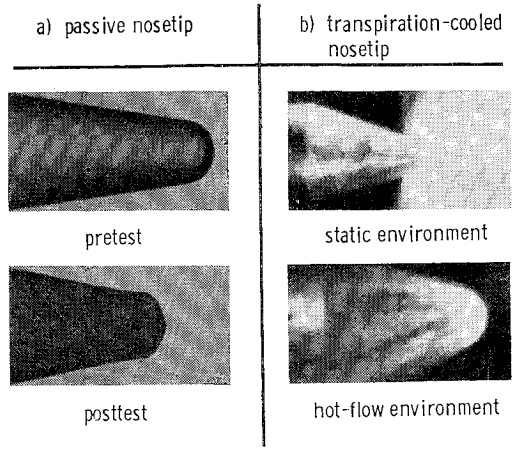

Fig. 1 Ablative and actively cooled nosetips.

Presented as Paper 69-96 at the AIAA 7th Aerospace Sciences Meeting, New York, January 20-22, 1969; submitted February 14, 1970; revision received September 23, 1970. The authors are pleased to acknowledge helpful discussions with J. H. Chin.

* Staff Engineer, Missile Systems Division.
† Graduate Study Engineer, Missile Systems Division. Member AIAA.
‡ Senior Mathematical Engineer, Missile Systems Division.

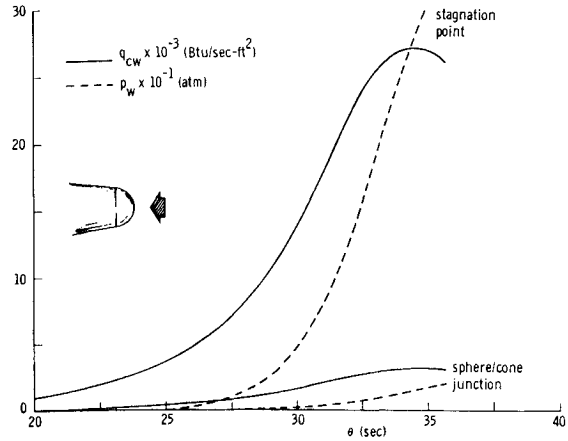

Fig. 2 Example re-entry environment for nosetip.

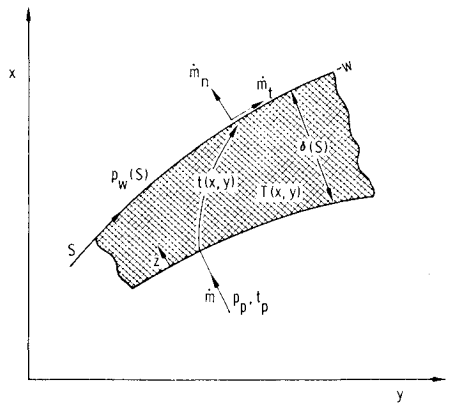

Fig. 4 Two-dimensional porous wall.

effects that are lacking in conventional transpiration theory and supporting experiments.[1] In view of the large time and spatial variations in external pressure and heat rate during re-entry (Fig. 2), the nosetip wall thickness and permeability must be nonuniform, coolant plenum pressure must vary with time, and coolant flow rates must be large to properly shield the nosetip down to impact. Although for incompressible coolants the total mass of coolant required is not large, the distribution and programing of this injectant is crucial since any local undercooling can result in rapid structural failure and because large local overcooling can effect vehicle dynamics and other performance characteristics.

Figure 3 demonstrates the practical consequences of two-dimensional coolant flow.[2] A hemispherical tip is shown with external surface pressure distributed as $\cos^2\phi$ and with coolant supplied from a single internal plenum chamber. If plenum pressure is high relative to external stagnation-point pressure, as in Fig. 3a, the coolant flow is effectively one-dimensional. This occurs at high altitudes in the subject application. For lower plenum pressures, as in Fig. 3b, large departures from unidirectional flow occur (low altitudes), especially in the immediate stagnation region. At still lower plenum pressures, as in Fig. 3c, the stagnation-point region can become starved of coolant because of strong two-dimensional effects. Both conditions (Figs. 3b and 3c) require two-dimensional solutions, because one-dimensional calculations are seriously nonconservative. In particular, the condition in Fig. 3c must be avoided because it represents a situation where external boundary-layer gases could be ingested with rapid thermal degradation of the nosetip matrix material.

This paper presents a calculation scheme for steady two-dimensional coolant and heat flow within a porous nosetip matrix. The model considers an incompressible coolant, variable coolant and matrix properties, variable coolant/matrix convection within the wall, and heat conduction in both coolant and matrix. This internal solution is coupled to the external heating environment by a simple exit-surface energy balance based on the assumption of complete coolant vaporization.§ A liquid rather than gas coolant is selected for analysis because its high energy blockage (heat of vaporization plus gaseous blowing) tends to minimize both volume and weight of the expulsion system needed to supply and regulate high-pressure coolant to the porous nosetip.

Analytical Model

The analysis considers the relations for momentum and energy exchange in a multidimensional porous medium and the assumptions made to simplify their solution in terms of the porous nosetip application. Some of these simplifications result from choosing an incompressible coolant (water) and in postulating that the coolant is supplied at a rate just sufficient to cause complete coolant phase change at the exit surface. The general two-dimensional problem is represented in Fig. 4 as an axisymmetric porous shell of finite curvature and nonuniform thickness δ. A coolant of unspecified mass

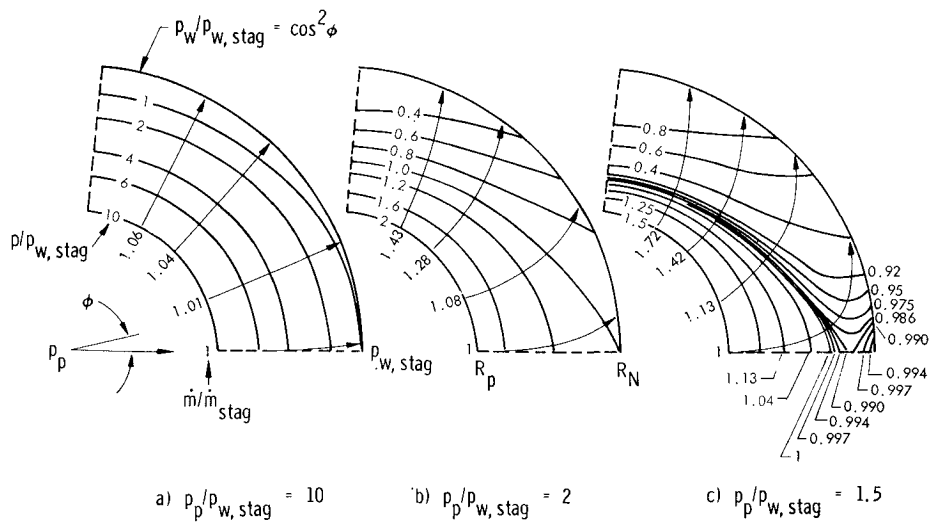

Fig. 3 Effect of plenum pressure on coolant flow in a hemispherical shell.

§ A more complete treatment of the exit-surface boundary condition with distributed coolant injection is given in Ref. 3.

flow rate $\dot{m}$ but known plenum pressure p_p and temperature t_p enters the wall at $z = 0$. Since exit-surface pressure p_w varies with distance S, the coolant path in the wall will curve as indicated, and the coolant will exit at $z = \delta$ with normal and tangential components $\dot{m}_n$ and $\dot{m}_t$.

The general momentum equation for mass transfer in a multidimensional permeable matrix penetrated by either compressible or incompressible fluids is[4]

$$-\text{grad } p = F(u)\mathbf{u} \tag{1}$$

where $\mathbf{u}$ denotes vector velocity. In Eq. (1)

$$F(u) = \alpha\mu_c + \beta\rho_c|\mathbf{u}|$$

where $\alpha\mu_c$ is the contribution to viscous pressure loss (laminar regime) and $\beta\rho_c|\mathbf{u}|$ represents inertial pressure loss at high coolant flow rates. Neglecting inertial effects reduces the above Forchimer flow to the well-known Darcy type for which mass flow rate is¶

$$\dot{\mathbf{m}} = \rho_c\mathbf{u} = -(\rho_c\Gamma/\mu_c) \text{ grad } p$$

where $\Gamma = 1/\alpha$ is permeability, a material characteristic determined by pore structure. The continuity equation for $\dot{m}$ is

$$-\text{div}(\dot{\mathbf{m}}) = d\rho_c/d\theta$$

Over-all system requirements for the nosetip application favor the use of liquid coolants. If internal coolant vaporization is not allowed, $d\rho_c/d\theta = 0$ and the mass continuity relation for Darcy flow becomes

$$\rho_c \text{ div}[(\Gamma/\mu_c) \text{ grad } p] = 0 \tag{2}$$

This differential equation can be solved directly (decoupled from energy considerations) if coolant viscosity μ_c is taken as constant, independent of temperature. In the design calculations μ_c was evaluated at 70°F. This choice was made because the major rise in liquid coolant temperature is confined to a zone near the exit surface. Moreover, the higher viscosity at 70°F tends to exaggerate the two-dimensional effect, and as such the minimum plenum pressure required to prevent stagnation-region coolant starvation is conservatively overestimated. The effect of inertial losses, which tend to become important at the high coolant flow rates required in reentry, is analyzed later in terms of a simpler one-dimensional model.

The differential equations describing energy conservation in the matrix and coolant are

$$\text{div } (k \text{ grad } T) - h'(T - t) = \rho c \partial T/\partial\theta \tag{3}$$

and

$$\text{div } (k_c \text{ grad } t) - \text{div } (\dot{m}c_c t) - h'(t - T) = \rho_c c_c \partial t/\partial\theta \tag{4}$$

These equations, which account for both matrix and coolant conduction, are coupled by virtue of matrix/coolant convective heat exchange. The enthalpy transport in Eq. (4) depends on $\dot{m}$ derived from Eq. (2). The transient storage terms are considered small relative to other energy components in the porous nosetip. As such $\partial T/\partial\theta = 0$ and $\partial t/\partial\theta = 0$ in Eqs. (3) and (4). The effect of this assumption is examined later by means of a one-dimensional energy solution.

The boundary conditions on the steady pressure field $p(x,y)$ from Eq. (2) are a known nosetip plenum pressure and boundary-layer edge pressure described by the exit-surface environment (Fig. 4):

$$\begin{aligned} p &= p_p \quad \text{at } z = 0 \\ p &= p_w(S) \text{ at } z = \delta \end{aligned} \tag{5}$$

Boundary conditions on the steady matrix and coolant temperature fields $T(x,y)$ and $t(x,y)$ from Eqs. (3) and (4) are

$$\begin{aligned} \partial T/\partial z = 0,\ t = t_p \text{ at } z = 0 \\ T = t = T_w(p_w) \text{ at } z = \delta \end{aligned} \tag{6}$$

The entrance face of the matrix is assumed to be adiabatic, and coolant conduction back into the plenum supply is neglected. Matrix and coolant temperatures are considered equal at the exit face. This is a consequence of assuming complete coolant vaporization at $z = \delta$, the common matrix/coolant temperature depending (through the vapor pressure law) on local exit-surface pressure p_w.

The instantaneous coolant mass flow rate $\dot{m}$ required to satisfy the vaporization boundary condition is determined by a quasi-steady, one-dimensional energy balance at the exit surface:

$$\Delta E = h_w(H_r - H_w) - \dot{m}(H_v - H_l) - k(\partial T/\partial z)_w - k_c(\partial t/\partial z)_w - \sigma\epsilon T_w^4 = 0 \tag{7}$$

Here $\Delta E < 0$ represents local overcooling, $\Delta E > 0$ local undercooling. The energy source term in Eq. (7) represents net hot-wall convective heat input balanced against coolant vaporization, matrix and coolant conduction, and surface reradiation as energy sinks. The blowing value of unit surface conductance h_w is obtained from Libby[5] for the laminar stagnation point corrected for foreign gas injectant as

$$h_w/h_o = f[(\dot{m}/h_o), (\overline{M}_a/\overline{M}_v)^{1/4}] \tag{8}$$

This is extended to other stations S/R_N by assuming local similarity for laminar flow. The corresponding value of h_w for turbulent flow is based on the correlation of Hidalgo.[6] The blowing effect in both cases is evaluated by using only the normal injection component $\dot{m}_n$. The wall enthalpy is taken to be that of coolant vapor, $H_w = H_v$; this is consistent with assuming large coolant flow rates and complete vaporization (no liquid film cooling). The vaporization component is based on the total vector quantity $\dot{\mathbf{m}}$. Coolant conduction and surface reradiation are generally small because $k_c \ll k$ and T_w is low with liquid coolants.

Design Method

Purpose of the two-dimensional model is to determine coolant pressure and mass flow distributions $p(x,y)$ and $\dot{m}(x,y)$ in the nosetip and resulting matrix and coolant temperature fields $T(x,y)$ and $t(x,y)$. These solutions, along with the exit-surface energy balance, provide information for structural design (coupled internal pressure and thermal stresses), and serve to determine the total coolant supply needed and the plenum pressure programing required for prescribed thermal shielding of the porous nosetip during reentry. Plenum pressure is, in turn, the independent variable for design of the coolant expulsion system.

Iteration Scheme

The exit-surface energy balance in Eq. (7) suggests that coupled momentum and energy solutions are needed because coolant flow depends on matrix and coolant temperatures. Neglecting the coolant conduction term $k_c(\partial t/\partial z)_w$ leaves $\dot{m}$ dependent only on T. In order to completely decouple the momentum and energy solutions, the matrix conductive flux at the exit surface $k(\partial T/\partial z)_w$ was evaluated for parametric

¶ The effect of vehicle deceleration on increasing $\dot{m}$ is neglected in the present study because this force is only about 0.01% of the coolant driving force across the nosetip during peak vehicle deceleration.

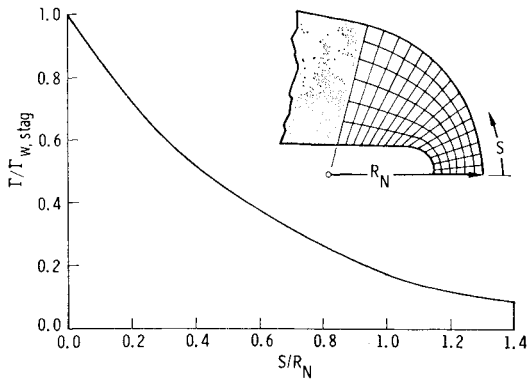

Fig. 5 Example nosetip permeability distribution.

values of $\dot{m}_n$ and T_w using a simplified one-dimensional energy solution. The following correlation for matrix conduction was obtained by curve fitting these approximate solutions over the range $0.1 \leq \dot{m}_n \leq 10$ lb/sec-ft^2 and $150 \leq T_w \leq 700$°F:

$$k(\partial T/\partial z)_w = 0.046\dot{m}_n^{0.69}T_w^{1.5} \quad (9)$$

Subsequent coupled solutions served to confirm that the error in $k(\partial T/\partial z)_w$ calculated from Eq. (9) is within $\pm 5\%$.

The nosetip design sequence is as follows: Given the flight trajectory plus nosetip size and shape, the cold-wall thermal environment and exit-surface pressure histories are established as in Fig. 2. Then preliminary distributions of wall thickness δ and permeability Γ are selected, based on structural sizing and porous-material fabrication technology. Next a design altitude is chosen at which to optimize δ and Γ. This optimization begins by first performing a decoupled momentum solution based on an initial guess at plenum pressure p_p. The results of this solution are used in the exit-surface energy balance to assess general adequacy of coolant distribution and to locate points of undercooling. Iteration on plenum pressure is carried out with the aim of eliminating local undercooling. This is accomplished by the simple perturbation

$$(\Delta p_p)_j = (\dot{m}_{\text{req}}/\dot{m}_{j-1})(\Delta p_p)_{j-1} \quad (10)$$

when $\dot{m}_{\text{req}}$ is obtained from Eq. (7), and repeating momentum solutions until the root $\Delta E = 0$ can be obtained by graphical interpolation. This results in a nosetip free of any local undercooling but generally overcooled at the design altitude. Next δ and/or Γ are changed with the aim of minimizing overcooling. Then with fixed δ and Γ, the plenum pressure required at other altitudes is calculated. Once the coolant flowfield history is established, energy solutions for the matrix temperature field can be calculated at all altitudes for which $\dot{m}(x,y)$ has been obtained.

Numerical Solution

Equations (2–4) were solved by explicit finite-difference formulations, using iterative relaxation of a two-dimensional, axisymmetric net. The porous nosetip was subdivided into 120 nodes for momentum solutions and 240 nodes for energy solutions (120 for matrix and a duplicate set of 120 for coolant). Convergence criteria for the relaxation procedure were selected as 0.1% on local residuals for momentum and 2% of maximum local flux for energy. Digital computer run times (Univac 1108) were approximately 0.5 min for momentum and 5 min for energy (matrix and coolant).

Table 1 Thermophysical data used in design calculations

	Matrix	Coolant
ρ	= 116 lb/ft^3	ρ_c = 62.3
c	= 0.6 Btu/lb-°F	c_c = 0.998
k	= 1×10^{-2} Btu/sec-ft-°F	k_c = 1×10^{-4}
β/α	= 1.9×10^{-5} ft	μ_c = 6.6×10^{-4} lb/sec-ft
$\Gamma_{w,\text{stag}}$	= 0.7×10^{-13} ft^2	t_p = 70°F

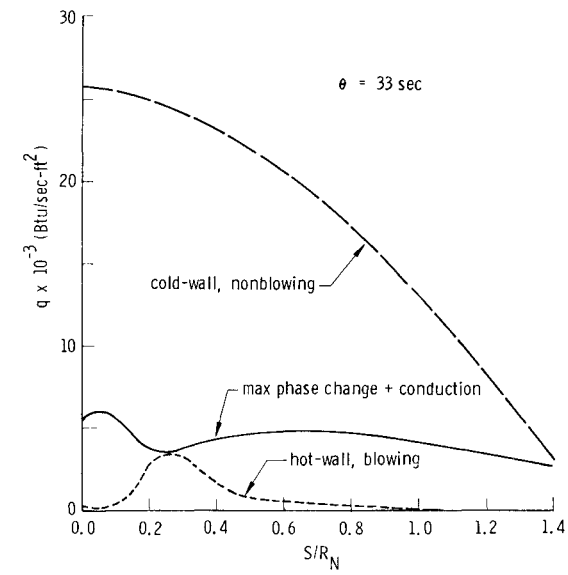

Fig. 6 Nosetip surface energy match at design altitude (water coolant).

Matrix and coolant properties selected for design exercise are tabulated in Table 1. Coolant properties in the momentum solutions were assumed constant (evaluated at 70°F), while temperature dependencies in c, k, ρ_c, c_c, k_c, and μ_c were included in the energy solutions. Although the assumption of constant coolant properties served to decouple the momentum and energy solutions, it is possible to improve on this by adopting an a priori distribution of $t(x,y)$ for property evaluations based on the known limits $T_w(S)$ and t_p.

Green[7] has correlated the resistance coefficients α and β from various spherical packed-bed data as $\beta/\alpha = 3.8 \times 10^{-2}/s(1 - P)$. Our own measurements on sintered powders indicate internal surface area of about $S = 4000$/ft. A

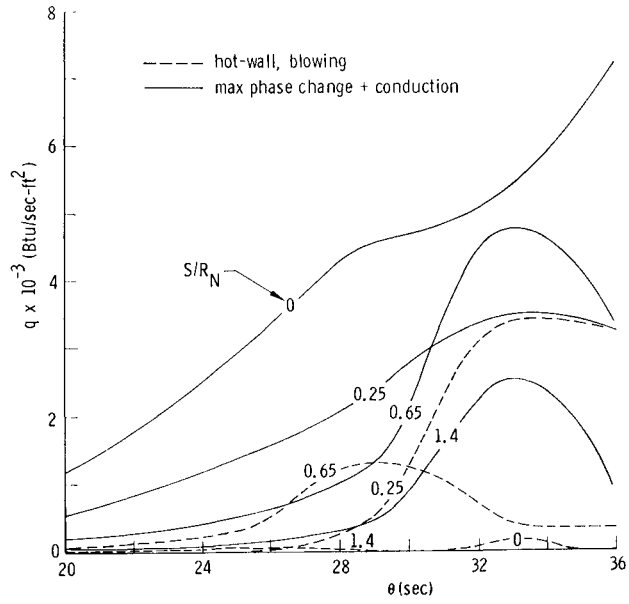

Fig. 7 History of nosetip surface energy match during re-entry.

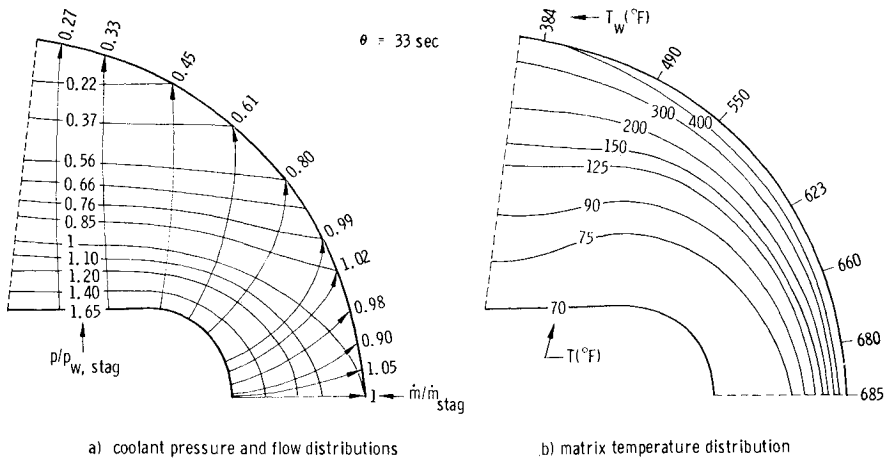

a) coolant pressure and flow distributions b) matrix temperature distribution

Fig. 8 Distributions of coolant pressure and mass flow plus matrix temperature at design altitude.

porosity of $P = 50\%$ gives the length parameter β/α tabulated in Table 1. This is taken as constant throughout the nosetip. However, the nosetip permeability is distributed as an exponential function of S as shown in Fig. 5, with the stagnation-point value tabulated in Table 1. Green has also reviewed convective heat-transfer measurements in a variety of porous matrices and correlated the data in terms of a coolant Stanton number $St_c = (h'/\dot{m}c_c)(\beta/\alpha)Pr_c^{2/3}$ as a function of coolant Reynolds number $Re_c = (\dot{m}/\mu_c)(\beta/\alpha)$. These correlated data have been curve fit to yield

$$St_c = 0.00434/Re_c^{0.44} \tag{11}$$

as the dependence of internal volumetric surface conductance h' on local mass flow rate $\dot{m}$.

Analysis Results

Water cooling of the forward hemispherical portion of a nosetip is considered for purposes of illustration. The design altitude is chosen as that corresponding with $\theta = 33$ sec. This is near peak heating (Fig. 2) and below the critical pressure of water (218 atm).

Figure 6 shows the surface energy match at the design altitude based on matrix thickness and permeability distributions from Fig. 5. Plenum pressure ratio at this altitude is $p_p/p_{w,\text{stag}} = 1.65$. The cold-wall, nonblowing convective heat load is strongly diminished by hot-wall and mass-injection effects. The remaining hot-wall, blowing heat load is accommodated by coolant phase change** plus matrix and coolant conduction. Evidently all nosetip stations are overcooled except $S/R_N = 0.25$ where the energy match is about optimum. Table 2 illustrates the relative contribution of the various exit-surface energy absorption terms in Eq. (7) at the design altitude. Gross overcooling at the stagnation point results in strong convective heat blockage (first term) compared to the balanced station $S/R_N = 0.25$. While vaporization energy absorption (second term) is comparable to the matrix conductive flux (third term), coolant conduction (fourth term) is several orders of magnitude less owing to low coolant conductivity (Table 1). Surface reradiation (fifth term) is negligible.

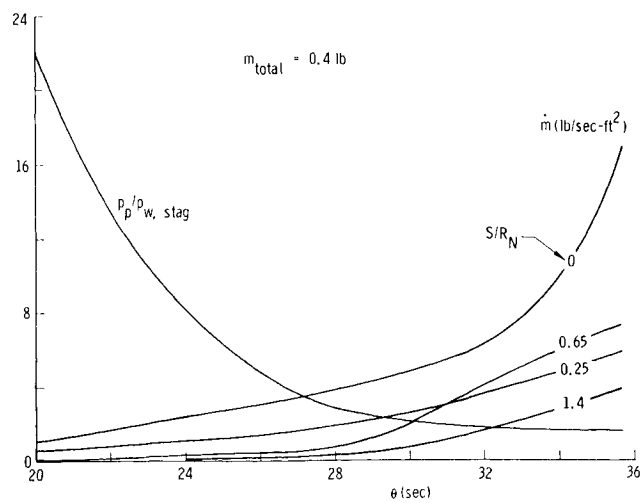

Fig. 9 History of plenum pressure and coolant flow rate during re-entry.

The over-all shielding mismatch shown in Fig. 6 can be improved by modifying the inner contour of the nosetip and/or changing permeability distribution.†† Figure 7 gives the history of energy match at four nosetip stations without changing δ or Γ. These distributions illustrate the inherent difficulty of optimizing coolant distribution through the entire re-entry heating pulse. The stagnation point $S/R_N = 0$ and sphere-cone junction $S/R_N = 1.4$ are both highly overcooled throughout re-entry. Station $S/R_N = 0.25$, although initially overcooled, becomes near critical at low altitude and remains so until impact. Station $S/R_N = 0.65$ is slightly undercooled for about three seconds and then becomes overcooled until impact. This small period of undercooling could cause local surface failure and subsequently result in progressive nosetip failure due to coolant flow perturbations. Evidently there is no unique combination of δ and Γ that will produce optimum cooling at all altitudes, since both the magnitude of cooling mismatch and the surface location of critical points changes with altitude.

Two-dimensional coolant pressure and mass flow-rate distributions plus the matrix temperature field at the design altitude are shown in Fig. 8. Although relatively constant, there is some oscillation in $\dot{m}/\dot{m}_{\text{stag}}$ along the forward face owing to differing rates of change in p_w plus δ and Γ. Beyond the 0.85 isobar, $\dot{m}/\dot{m}_{\text{stag}}$ falls off monotonically, illustrating that increasing wall thickness coupled with decreasing permeability finally overcomes external pressure decay along the nosetip. The matrix temperature field exhibits strong gradients near the exit surface owing to large coolant flow rates. This is quite pronounced over the complete forward region

** The term "max phase change" in Fig. 6 implies that all coolant is potentially available for vaporization heat absorption. Actually only a portion of $\dot{m}$ would be available since with overcooling the surface temperature drops and a finite film thickness develops. In this instance the vaporization component depends on the dynamics of the liquid film.

†† Although not considered here, Γ could be made to vary with both S and z.

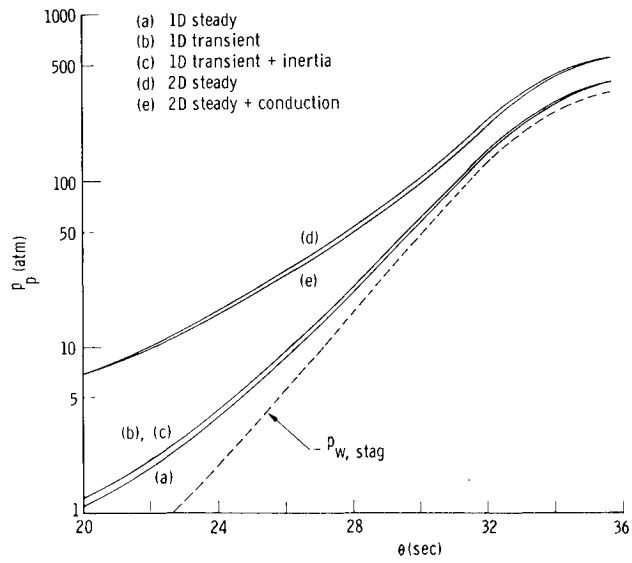

Fig. 10 Plenum pressure histories based on one- and two-dimensional solutions.

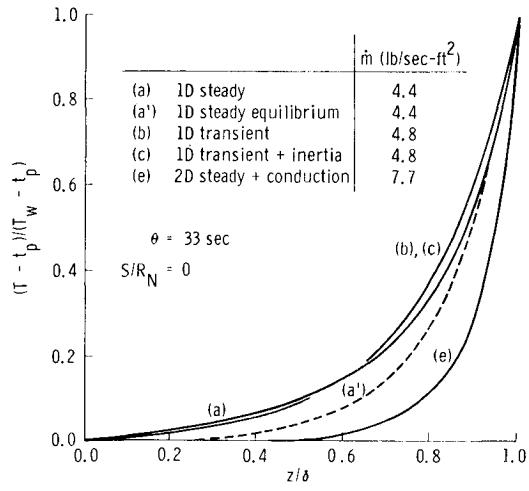

Fig. 11 Stagnation-line matrix temperature profiles based on one-dimensional energy solutions.

of the nosetip. Although not shown in Fig. 8b, the matrix/coolant temperature difference is not large, the coolant temperature being about 10% lower in the steep-gradient region just below the exit surface.

Figure 9 gives the history of nosetip plenum pressure and surface coolant injection rates during re-entry. Comparison with Fig. 3 suggests that when $p_p/p_{w,stag} \geq 10$ the coolant flow is essentially radial, and as such $\dot{m}$ could be predicted by a one-dimensional solution down to altitudes corresponding to $\theta = 23$ sec. Beyond this time two-dimensional calculations are needed to avoid coolant starvation in the stagnation-point region and/or local undercooling. The critical pressure of water is exceeded just past the design altitude (33 sec). At pressures exceeding the critical point, surface vaporization was no longer considered to contribute to total energy absorption, and surface temperature plus wall enthalpy were held constant at their critical values. Integration of the local coolant flow rates over the nosetip surface gives the total mass of water required as 0.4 lb, only 180 cm³.

Plenum pressure histories calculated by various models are compared in Fig. 10. A one-dimensional solution was developed that was analogous to the two-dimensional model except for retention of the inertial term in the momentum equation and the transient term in the energy equations. This model was used to calculate plenum pressure requirements based on nosetip stagnation-point conditions. Curve a of Fig. 10 shows plenum pressure according to the simplest model, namely one-dimensional, axisymmetric with viscous effects only. Curve b adds the effect of transient energy storage in matrix and coolant. The transient effect is evidently not very large, but its neglect in predicting p_p is nonconservative.‡‡ Inertial effects were included by solving Eq. (1)

Table 2 Energy partition at exit surface (33 sec)

S/R_N	0	0.25
$h_w(H_r - H_w)$	300	3415
$\dot{m}(H_v - H_l)$	2060	1340
$k(\partial T/\partial Z)_w$	3225	2090
$k_c(\partial t/\partial z)_w$	35	27
$\sigma\epsilon T_w^4$	1	1
ΔE (Btu/sec-ft²)	−5021	−43

‡‡ Early in re-entry the storage term is comparable to the matrix conductive flux at the exit surface, while near impact it is only 1% of this term.

complete with inertial pressure loss. As seen by curve c, this did not have a detectable effect on the one-dimensional transient solution. Curves a, b, and c in Fig. 10 serve to suggest that both transient and inertial effects can be neglected in the two-dimensional solutions.

Curves d and e in Fig. 10 represent two-dimensional calculations with and without matrix conduction effects in the surface energy balance, Eq. (7). Although matrix conduction is substantial (Table 2), its equivalent energy accommodation can be obtained by added blowing from the relatively small increase in plenum pressure indicated by curve d. Neglecting matrix conduction (plus reradiation) serves to decouple the momentum and energy equations, resulting in a considerable reduction in design time with only a minor penalty in overdesign [curve d].

Curve e emphasizes the serious underdesign that would accompany the use of conventional one-dimensional transpiration theory. The severe pressure gradient along the nosetip serves to drain coolant away from the high-pressure stagnation point. Since no such drain is identified by the one-dimensional treatment, the plenum pressure requirements are grossly underestimated, and moreover there is a real possibility of coolant starvation and ingestation of high-temperature boundary-layer gases if p_p is derived solely from one-dimensional models.

Structural design of porous nosetips requires, in addition to internal pressure fields, an accurate assessment of matrix temperature gradients. Although temperature levels with liquid coolants are low, the high coolant flow rates required generate steep temperature gradients at the exit surface (Fig. 8b). Prediction of these gradients by various models is compared in Fig. 11 for conditions corresponding to the stagnation point at the design altitude. Curve a is the one-dimensional, axisymmetric, steady-state solution referred to in Fig. 10. Curve a′ in Fig. 11 represents the limiting case of matrix/coolant thermal equilibrium for which the exact solution in cylindrical geometry is[8]

$$(T - t_p)/(T_w - t_p) = [R/(R_p + \delta)]^{\dot{m}c_c R_N/k} \qquad (12)$$

The perfect matrix/coolant thermal coupling results in lowest one-dimensional matrix temperatures. Once again, curves b and c suggest that inertial and transient effects are generally small. The slight increase in $\dot{m}$ results from using an exact surface energy balance for the transient solutions. Curve e represents the two-dimensional profile at $S/R_N = 0$ from Fig. 8b. Matrix temperatures are lowest in this case not because of significant lateral energy drain but because the $\dot{m}_{stag}$ is large in order to prevent undercooling away from the stagnation point. This leads to steep temperature

gradients at $z = \delta$ and a serious underestimate of thermal stress if a one-dimensional solution is employed.

The foregoing results suggests an abbreviated design method suitable for rapid engineering parametric studies: estimate $p(x,y)$ and $\dot{m}(x,y)$ from decoupled, steady, two-dimensional, viscous momentum solution and decoupled, quasi-steady, one-dimensional surface energy balance, approximating $t(x,y)$ for evaluation of coolant properties in the former, plus neglecting coolant conduction and approximating matrix conduction [Eq. (9)] in the latter. Evaluate $T(x,y)$ from two-dimensional, steady, nonequilibrium solution using the local two-dimensional $\dot{m}$. An equivalent one-dimensional energy solution may be used only where coolant flow is approximately radial (sphere/cone junction).

Conclusions

An analysis method for steady, two-dimensional transpiration cooling with incompressible coolants has been developed and exercised in terms of the hyperthermal re-entry nosetip problem. Two-dimensional effects in coolant flow are found to be important for assessing internal coolant distribution and for determining the coolant plenum pressure history required to achieve adequate nosetip thermal shielding. The conventional one-dimensional theory can lead to local coolant starvation, an underestimate of internal matrix pressure and thermal stress, and an underdesigned coolant expulsion system.

The nosetip application highlights an inherent difficulty in optimizing thermal shielding throughout exposure to a transient re-entry environment. Off-optimum design results in transient patterns of local overcooling and associated departure from the simple vaporization boundary condition.

Future work on the problem should include a more comprehensive treatment of the exit-surface boundary condition, such as two-dimensional boundary-layer effects due to discrete injection jets and film cooling associated with local overcooling.[3] Studies of coolant phase change within the porous wall are needed, including an assessment of instabilities occurring with flashing to two-phase flow. The highly coupled problem arising with the use of compressible coolants warrants attention for possible nosetip cooling applications. A theory for compressible coolants would also impact the related problem of two-dimensional pyrolysis gas flow in a passive charring ablator exposed to high surface pressure gradients.

References

[1] Kelley, J. B. and L'Eouyer, M. R., "Transpiration Cooling—Its Theory and Application," Rept. TM-66-5, June 1966, Purdue Univ., Lafayette, Ind.

[2] Schneider, P. J. and Maurer, R. E., "Coolant Starvation in a Transpiration-Cooled Hemispherical Shell," *Journal of Spacecraft and Rockets*, Vol. 5, No. 6, June 1968, pp. 751–752.

[3] del Casal, E. P., "The Effects of Multidimensional Flow Through Porous Matrices in Mass Transfer Cooling," AIAA Paper 69-149, New York, Jan. 1969.

[4] Scheidegger, A. E., *The Physics of Flow Through Porous Media*, MacMillan, New York, 1960.

[5] Libby, P. A., "The Homogeneous Boundary Layer at an Axisymmetric Stagnation Point With Large Rates of Injection," *Journal of the Aeronautical Sciences*, Vol. 29, No. 1, Jan. 1962, pp. 48–60.

[6] Hidalgo, H., "Ablation of Glassy Materials Around Blunt Bodies of Revolution," *Journal of the American Rocket Society*, Vol. 30, No. 9, Sept. 1960, pp. 806–814.

[7] Green, L. Jr., "Heat, Mass and Momentum Transfer in Flow Through Porous Media," ASME Paper 57-HT-19, 1957, Univ. of Pennsylvania.

[8] Koh, J. C. Y. and del Casal, E. P., "Temperature and Pressure Distribution for Fluid Flow Through a Porous Wall of Cylindrical and Spherical Bodies," D2-24105-1, Jan. 1966, The Boeing Co., Seattle, Wash.